IEEE Access
Multidisciplinary ⋮ Rapid Review ⋮ Open Access Journal

Received 29 July 2022, accepted 12 August 2022, date of publication 18 August 2022, date of current version 25 August 2022.

Digital Object Identifier 10.1109/ACCESS.2022.3199754

RESEARCH ARTICLE

A Wideband Antenna for mm-Wave Antenna-in-Package Application

XUESONG ZHANG, QIAN WANG, (Member, IEEE), AND JIAN CAI, (Senior Member, IEEE)
School of Integrated Circuits, Tsinghua University, Beijing 100084, China

Corresponding author: Xuesong Zhang (zhangxs15@mails.tsinghua.edu.cn)

ABSTRACT Antenna-in-Package has been widely applied for millimeter-wave systems that integrate the MMIC chip and antenna into one package. For organic substrate Antenna-in-Package solutions, probe feeding and aperture-coupled feeding patches are generally used as radiation units. In this work, a patch antenna is proposed using coupled resonation; a wideband, high-gain and compact 3-D antenna package integration is realized. Equivalent circuit model is analysed for the coupled structure. $\boldsymbol{\lambda/4}$ coupled line is adopted for impedance matching, the whole antenna is designed on the same thick radiation patch substrate, with less organic substrate lamination layers. For millimeter-wave Antenna-in-Package structures, vias are generally used for vertical interconnections, which function well in the lower millimeter-wave frequency range. For operation frequency higher than 100 GHz, design difficulties may be encountered for via interconnection, with performance degeneration on impedance matching and transmission loss. In our work a H-shaped slot is integrated instead of vias on an organic substrate, realizing a high frequency and wideband mm-wave transition. An interconnection structure is also adopted to convert a microstrip line to differential microstrip line in the feeding network. Antenna prototype with 2×4 radiation array is designed for verification purpose at 20 GHz frequency range with simulated bandwidth of 23%. The prototype is fabricated with separate PCB boards assembled with screws; measured antenna gain is 12.7 dBi - 13.5 dBi. The proposed structure provides a wideband and low-loss solution for potential higher frequency mm-wave Antenna-in-Package applications.

INDEX TERMS Antenna-in-package (AiP), coupling feed, millimeter-wave (mm-wave), wideband.

I. INTRODUCTION

Antenna-in-Package (AiP) has been widely adopted in the mm-wave system, with application frequencies covering the entire mm-wave range (30-300 GHz) [1], [2]. The main application scenarios include high data rate wireless communication, and high accuracy distance and position sensor [3]. For both applications, a wide bandwidth is desirable, which is limited by available frequency band. In our project, an antenna prototype is proposed for wide bandwidth realization; the antenna is designed and fabricated under a relatively low 20 GHz frequency range for verification purposes.

MMIC chip in the AiP system can be attached to the antenna substrate with chip pad connected by wire bonding or solder bumping, which introduce parasitic parameters. Another method is to have the chip embedded into substrate, using fan-out Redistribution Layers (RDL) for interconnection [4], [5], which has low parasitic parameters and is the most suitable for mm-wave system integration. For an AiP system, two distribution wire networks are required; one for chip pad interconnection, another for antenna feeding network. Patterning of the two wire networks on two separate metal layers is preferable for large-sized antenna array realized with confined package dimension. The ground plane can be used to isolate the antenna on one substrate surface from the MMIC chip on another surface, forms a compact three-dimensional integration. LTCC and organic substrates are generally used for mm-wave antenna design, in our project, an organic substrate is adopted due to the low cost and low dielectric constant with relatively large pattern size, which is suitable for mm-wave antenna applications.

Generally, the bandwidth of a rectangle microstrip radiation patch is only approximately 1% to 7%. Various techniques for bandwidth enhancement can be adopted, such as

The associate editor coordinating the review of this manuscript and approving it for publication was Hussein Attia.

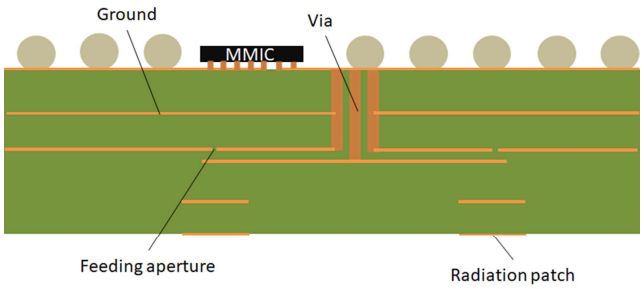

FIGURE 1. Antenna-in-Package with aperture-coupled feed.

adding slots to the patch [6], [7], using stacked patches or superstrate [8], [9], and proximity coupling [10]. Aperture-coupled feed is the most adopted method due to its convenience in design and fabrication process, as shown in Fig.1. For AiP structure adopting aperture coupling, dual ground planes may be needed to avoid electromagnetic wave backward radiation of the aperture, as in Fig.1. The redundant metal layer may add to fabrication cost, which increases with the number of layers. For the AiP structure with MMIC die embedded into organic substrate [4], [5], a flexible and compact antenna-package codesign can be acquired. If probe feed is adopted, no redundant ground plane is needed. Generally, the probe-fed patch antenna shows a limited bandwidth, L-shaped probe can be adopted for bandwidth enhancement [11], [12].

The bandwidth of the antenna can also be improved by inserting filtering function into the feeding path. With patch antenna modelled by parallel resonance RLC circuit, a theoretically available maximum impedance bandwidth B_m under arbitrarily approachable matching network is given by the Bode-Fano criterion [13]

$$B_m = \frac{1}{Q}\frac{\pi}{\ln\left\{\frac{S+1}{S-1}\right\}} \tag{1}$$

Here S is equal to VSWR, and Q is the quality factor of the RLC circuit. The Bode-Fano criterion reveals that the impedance matching bandwidth can be improved by modifying the matching network. Filter antenna is the structure where filter is inserted into the feeding path for integration of functions such as high out-of-band suppression or skirt roll-off rate [14], [15], [16]. A convenient design approach is to use the Q value of the radiation unit as a load quality factor, taking the form of a standard filter for design, which however does not consider bandwidth enhancement [14], [16]. In our project, wideband performance is realized by using a split patch with coupling feed. As the design goal is merely bandwidth improvement, an intuitive analysis is presented here instead.

Via interconnection is generally applied for vertical signal transition, and transmission line can be formed by vias [17] with a proper characteristic impedance. Care should be taken during impedance matching as the via pads introduce

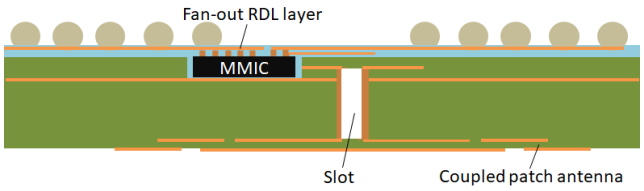

FIGURE 2. Proposed Antenna-in-Package structure.

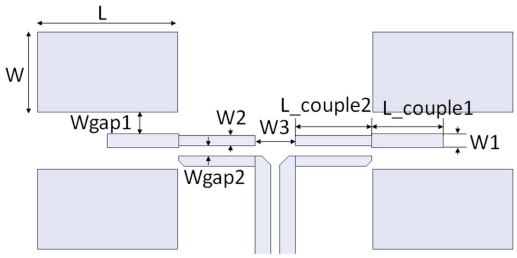

FIGURE 3. Proposed wideband patch antenna using coupled feeding structure.

parasitic capacitors. Aiming at applications on higher mm-wave frequency range, our work adopts a right-angle transition slot instead of via interconnection. Conversion structures are also designed to connect the microstrip line (MS line) into differential MS line in the feeding network.

II. WIDEBAND COUPLED FEEDING ANTENNA

The Antenna-in-Package topology in our work is illustrated in Fig.2. The MMIC die is embedded in organic substrate, with fan-out RDL layers for chip pad interconnection. A vertical transition slot is designed instead of vias, coupling the microstrip lines on the top and bottom surfaces of the substrate board.

A. ANTENNA DESIGN

The coupled feeding antenna is shown in Fig.3, which contains a pair of microstrip patches, each microstrip patch is split into two halves, coupled by the feed line in between, forming a balanced coupling that reduces radiation pattern deformation and suppresses cross polarization. The coupled patch is fed by a $\lambda/4$ coupled line with length L_couple2, which can be patterned on the same thick substrate with the patch antenna, a wideband structure can be formed with fewer substrate layers. In comparison, if a microstrip line is used for feeding on the same thick substrate, the transmission mode of the MS line can deteriorate with a large surface wave leakage [18]. Fig.3 appears like a two-stage $\lambda/4$ coupled line bandpass filter, yet the coupling between $\lambda/4$ line with length L_couple1 and the radiation patch is loose, and loss exists on both the patch and the $\lambda/4$ line, which is caused by radiation and surface wave and brings resistive loads on both sides of the coupled stage.

The design parameters in the HFSS simulation are listed in Table 1. The excitation wave port is applied on a differential MS line at the input of Fig.3. Resulted S11 is

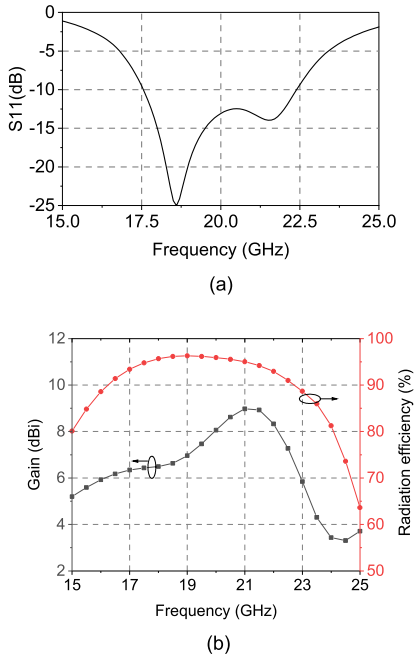

FIGURE 4. (a) Simulated input reflection coefficient (b) Gain and radiation efficiency versus frequency.

TABLE 1. Dimensions of the coupled antenna.

Parameter	L	W	Wgap1	L_couple1	L_couple2
Value(mm)	3.15	1.8	0.49	1.605	1.72
Parameter	W1	W2	W3	Wgap2	
Value(mm)	0.3	0.23	0.9	0.23	

shown in Fig.4(a) with differential MS line de-embedded. The bandwidth for −10 dB input reflection coefficient is 17.6-22.4 GHz. Fig.4(b) depicts the gain and radiation efficiency versus frequency; in-band gain is 6.4 dBi - 9 dBi with radiation efficiency of over 93%.

B. EQUIVALENT CIRCUIT MODEL

Analysis of the radiation unit is established with two λ/4 coupling parts; the first part of length L_couple1 is the coupled resonator, and the second part of length L_couple2 forms impedance transformation. An RLC parallel network models the radiation patch in the coupled resonator. The open-circuited λ/4 feed line with length L_couple1 can be modelled by an RLC series network, forms a series-to-parallel coupled resonator along with the radiation patch. The equivalent circuit is shown in Fig.5(a), where $R_1L_1C_1$ and $R_2L_2C_2$ are equivalent circuits for the radiation patch and the λ/4 coupled feed line, R_L is the source impedance, C_m is the mutual capacitance between C_1 and C_2, and k_m is the magnetic coupling coefficient between L_1 and L_2. Here coefficient k_m is used instead of mutual inductance L_m for the convenience of

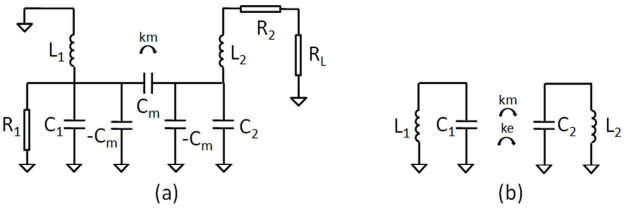

FIGURE 5. (a) Equivalent circuit model for the coupled feeding patch antenna (b) Simplified lossless circuit model.

FIGURE 6. (a) Split radiation patch simulation (b) Coupled resonator simulation.

schematic formation, which is readily managed by cadence circuit simulation.

Device parameters in the equivalent circuit can be extracted from HFSS simulation. The split patch is simulated as in Fig.6(a), with two lumped ports applied, the total input impedance Z_i can be calculated as

$$Z_i = \frac{1}{(\frac{1}{Z_{11}+Z_{12}} + \frac{1}{Z_{21}Z_{22}})} \tag{2}$$

The parallel *RLC* values are extracted to be $R_1 = 120\Omega$, $C_1 = 374$fF, $L_1 = 0.169$nH. Series RLC circuit of the λ/4 feeding line is also extracted from HFSS simulation, with resulted value $R_2 = 6.9\Omega$, $C_2 = 78$fF, $L_2 = 0.62$nH. The coupling of the radiation patch and the λ/4 line is simulated as in Fig.6(b). The split patch and the λ/4 line are patterned on the upper surface of the top and middle PCB boards, respectively, as illustrated in Fig.18. The coupled resonance peak appears on the real part of the input admittance curve.

The circuit of Fig.5(a) shows damped oscillation caused by R_1, R_2, and R_L when excited. Designed intrinsic resonance frequencies of L_1C_1 and L_2C_2 are roughly equal, which are pulled by coupling, and the resulted resonation frequencies are separated. For evaluation purposes, lossy devices including R_1R_2 and R_L can be omitted, with the assumption of unchanged resonance frequencies. The resulted lossless network is shown in Fig.5(b) and is the same as the coupled resonator in [19]. The total coupling coefficient k can be calculated as follows:

$$k = \pm\frac{1}{2}\left(\frac{\omega_{02}}{\omega_{01}} + \frac{\omega_{01}}{\omega_{02}}\right)\sqrt{\left(\frac{\omega_2^2-\omega_1^2}{\omega_2^2+\omega_1^2}\right)^2 - \left(\frac{\omega_{02}^2-\omega_{01}^2}{\omega_{02}^2+\omega_{01}^2}\right)^2} \tag{3}$$

Here $k = k_e + k_m$, k_e and k_m are the electrical and magnetic coupling coefficients, ω_{01} and ω_{02} are the intrinsic resonant frequencies of the two uncoupled resonators, which are 20 GHz and 22.9 GHz in our design. ω_1 and ω_2 are

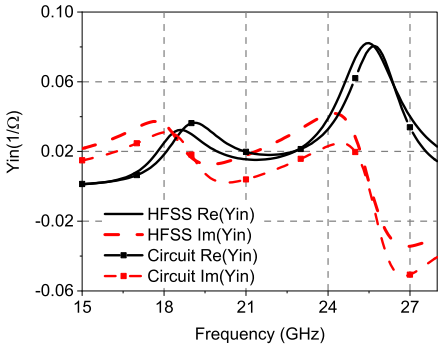

FIGURE 7. Curve-fitted input admittance for the equivalent circuit and the HFSS model.

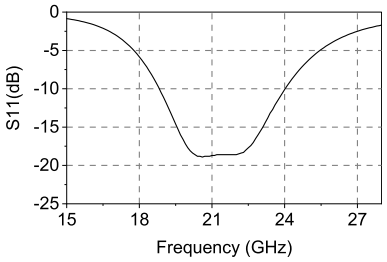

FIGURE 8. Simulated S11 of the equivalent circuit.

the coupled resonation frequencies, which are 18.6 GHz and 25.5 GHz, respectively. Using (3), the coupling coefficient k is calculated to be ± 0.276. C_m and k_m in Fig.5(a) can be estimated through curve fitting between the circuit simulation and the HFSS simulation results, with restriction $k_e + k_m = C_m/\sqrt{C_1C_2} + L_m/\sqrt{L_1L_2} = \pm k$. Impedance R_L in Fig.5(a) is changed with psin source during circuit simulation. The resulted values are $C_m = 57$fF, $k_m = 0.062$.

As the radiation and surface wave created by the $\lambda/4$ line is suppressed when coupled to the patch, the R_2 value of the $\lambda/4$ line differs with and without coupling. Fig.7 illustrates the final fitting curve, where the R_2 value is adjusted from 6.9 Ω to 3 Ω. Although multiple approximations have been taken, the input admittance of the equivalent circuit is generally in agreement with the HFSS results.

The circuit model can be conveniently adopted to reflect the bandwidth enhancement performance. Setting the psin source impedance to 39 Ω, the input reflection coefficient can be simulated by cadence sp analysis with the result shown in Fig.8, which has a -10 dB bandwidth of 23.8%, roughly indicating the bandwidth enhancement ability of the coupling structure. A 100 pH inductance is added in series with the psin source for better impedance matching during simulation; the inductance value is small compared with L_2, and can be formed by adjusting the feed line length.

The coupled line with length L_couple2 in Fig.3 is a two-port network, as shown in Fig.9, which provides wideband impedance matching. The Z parameters of the network are as

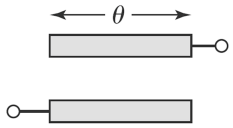

FIGURE 9. Two-port network formed by $\lambda/4$ coupled line.

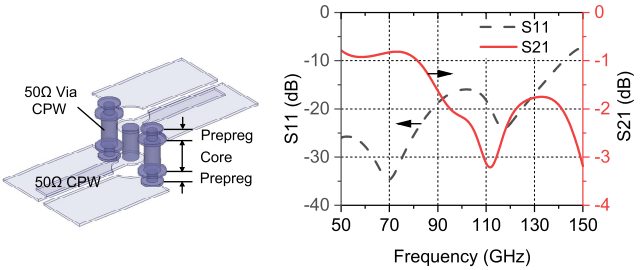

FIGURE 10. Simulation of CPW line structure formed by vias.

follows:

$$Z_{11} = Z_{22} = -\frac{j}{2}(Z_{0e} + Z_{0o})\cot\theta \tag{4}$$

$$Z_{12} = Z_{21} = -\frac{j}{2}(Z_{0e} - Z_{0o})\csc\theta \tag{5}$$

where Z_{0e} and Z_{0o} are the characteristic impedances of the even and odd modes, respectively. For two-port network, assuming port2 is loaded by impedance Z_L, the input impedance seen at port1 is

$$Z_{in} = Z_{11} - \frac{Z_{12}Z_{21}}{Z_L + Z_{22}} \tag{6}$$

For $\lambda/4$ coupled line, $\theta = \pi/2$, Z_{in} can be calculated from (4), (5) and (6) as

$$Z_{in} = \frac{(Z_{0e} - Z_{0o})^2}{4Z_L} \tag{7}$$

In our design, Z_{0e} and Z_{0o} are 140 Ω and 55 Ω, respectively; the characteristic impedance of the differential MS line at the input of Fig.3 is 93 Ω, with a single-ended impedance 46.5 Ω. Using this value as Z_L, Z_{in} can be calculated as 39 Ω, which has been mentioned for the simulation in Fig.8. The θ value in Fig.9 varies within $\pi/10$ over the entire operation frequency band; thus, Z_{in} does not change significantly in the band and forms a wideband impedance transformation. It should be noted that the calculation above is based on the assumption of ideal open-circuit ports of the $\lambda/4$ coupled line in Fig.9, which in fact have parasitic capacitors. Equation (7) is not accurate enough to be adopted in the design and is used only for principle analysis.

III. ANTENNA ARRAY DESIGN

A. VERTICAL TRANSITION STRUCTURE

Generally, vias are adopted for vertical interconnections in AiP substrate. Transmission line can be formed by three parallel vias as shown in Fig.10; for simulation, the core layer thickness of the organic substrate is set to be 300 μm, with

TABLE 2. Size of the vertical transition structure.

Parameter	W1	L1	W2	L2	Ls	W3
Value(mm)	0.8	2	0.8	3.5	1.55	0.2

100 μm prepregs laminated on both surfaces. Via diameters in the core layer are 150 μm, with via pad diameters 250 μm and center spacing 300 μm. For the prepreg layers, diameters of the vias and via pads are set to be 100 μm and 200 μm, respectively. The dielectric constant used in simulation is 3.3. The vertical coplanar waveguide (CPW) formed by the three vias has a characteristic impedance of 50 Ω according to HFSS simulation, connects to CPW lines on the two substrate surfaces, which have characteristic impedance of 50 Ω, too. Simulation shows a wideband impedance matching can be obtained when frequency is lower than 80 GHz, and the insertion loss is within −1 dB. When the frequency exceeds 80 GHz, the transmission performance starts to degenerate. For frequency higher than 100 GHz, S21 will attenuate to be lower than −2 dB, which shows that via interconnection has difficulties for applications over 100 GHz.

In our work a right-angle transition H-shaped slot is adopted instead, as shown in Fig.11. An antenna prototype is realized using three RO4350B boards with thicknesses 338 μm, 762 μm, and 338 μm respectively. The H-shaped slot penetrates the middle PCB board with the sidewall electroplated. The MS lines on top PCB board are formed to feed the antenna array, another MS line on the bottom PCB board is used to connect to the MMIC pad, with a forked-shape for better coupling.

The antenna prototype is designed to operate under 20 GHz with target bandwidth of 17%. The slot depth in Fig.11 is 762 μm, which is far lower than the operating wavelength; thus, the design can follow the concept of aperture coupling. The slot also forms a vertical waveguide, where care should be taken so that the cut-off mode of the waveguide does not cause severe transmission loss. The MS lines pass across the slot with a stub length of nearly $\lambda/4$. Transmission loss due to radiation leakage can be severe as the slot is basically an antenna element. With electric fields on four arms of the H-shaped slot in opposite directions, radiation cancellation can be achieved in the boresight direction, which lowers transmission loss. Parameters of the slot transition structure are listed in Table 2. Fig.12 shows the simulated results, the single-ended insertion loss of the differential structure is below −3.62 dB, which corresponds to a total loss of −0.62 dB. Input reflection coefficient in the band is lower than −16 dB.

For comparison purpose, a H-shaped slot with operation frequency above 100 GHz is also designed as in Fig.13, the size parameters which have been marked in Fig.11(b) are *W1*=0.2 mm, *L1*=0.4 mm, *W2*=0.2 mm, *L2*=1.2 mm, *W3*=0.1 mm, *Ls*=0.32 mm. The slot depth is 300 μm, thickness of MS line dielectric is 100 μm. Simulated input reflection coefficient is lower than −15 dB in the frequency

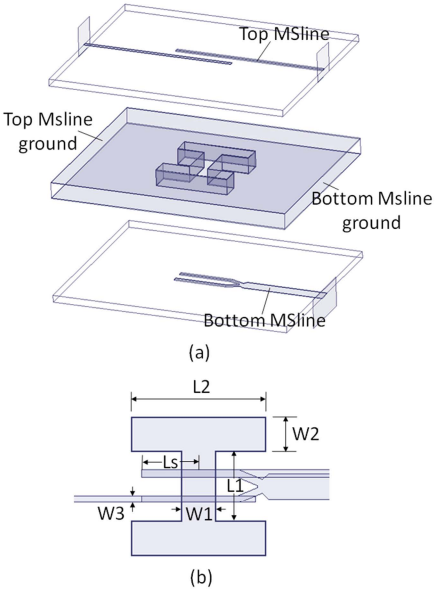

FIGURE 11. (a) Vertical transition structure (b) Top view.

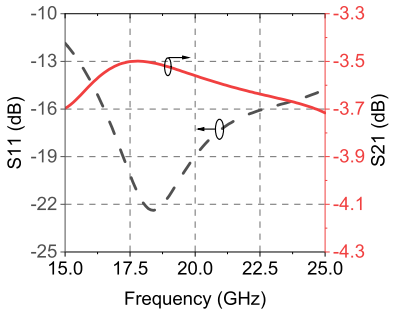

FIGURE 12. Simulated scatter parameters for vertical transition structure.

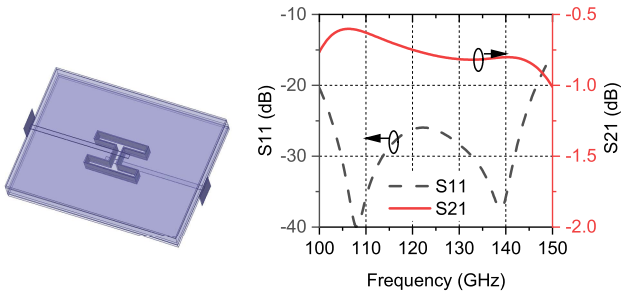

FIGURE 13. Simulation of H-shaped slot transition structure designed for 100-150GHz frequency range.

range 100 GHz - 150 GHz, the insertion loss is within −1 dB, as in Fig.13. The H-shaped slot shows a better performance compared with Fig.10, due to the aperture resonation feature.

B. CONVERSION BALUN

The conversion balun connects the differential MS line in Fig.3 to the MS line of the vertical transition structure on the top PCB board in Fig.11. The design is shown in Fig.14.

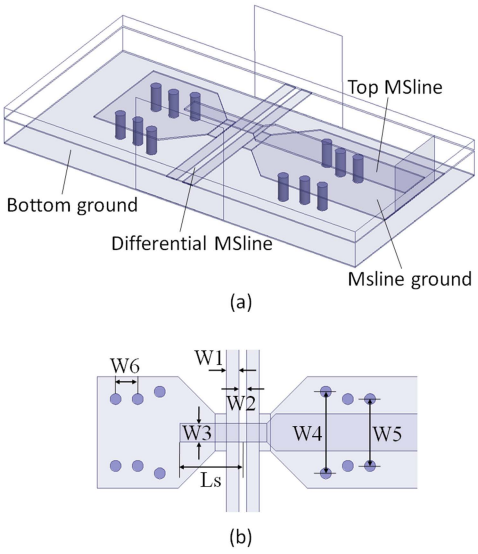

FIGURE 14. (a) Differential MSline to MSline conversion (b) top view.

TABLE 3. Size of the conversion balun.

Parameter	W1	W2	W3	W4	Ls	W5	W6
Value(mm)	0.35	0.2	0.5	2.2	1.7	1.8	0.6

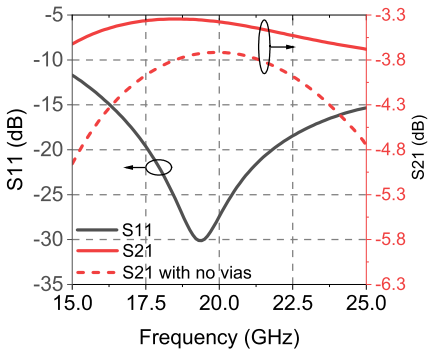

FIGURE 15. Simulated scatter parameters for the conversion balun; dashed line is for S21 with no vias.

The MS line with width *W3* passes across the differential MS line with stub length *Ls* about $\lambda/4$ for impedance matching. Ground vias are arranged to form a substrate integrated waveguide (SIW) between the MS line ground and the bottom ground, as in Fig.14. The leakage of electromagnetic waves between the two ground layers is choked because the TE10 cut-off frequency of the SIW is far beyond the operation frequency. Design parameters are listed in Table 3. Simulation is performed with three wave ports applied on the MS line and differential MS line; the results are shown in Fig.15. Single-ended insertion loss is nearly −3.5 dB, and the total insertion loss is −0.5 dB. A wide bandwidth is acquired, which is approximately 43% with input reflection coefficient lower than −15 dB. The insertion loss will degenerate by more than 0.3 dB if the ground vias are not used, as shown in Fig.15.

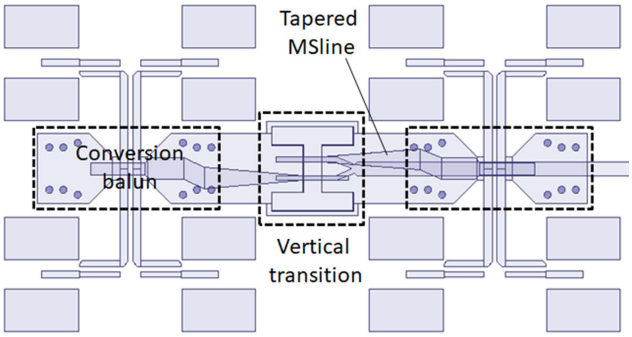

FIGURE 16. Diagram of 2 × 4 antenna array.

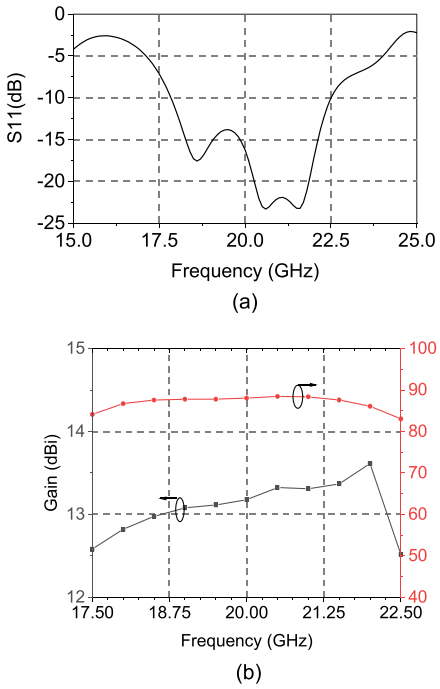

FIGURE 17. (a) Simulated input reflection coefficient and (b) Gain and radiation efficiency of antenna array.

C. ANTENNA ARRAY

The 2 × 4 antenna array is designed as shown in Fig.16. $\lambda/2$ tapered MS line is inserted between the right-angle transition structure and the conversion balun for impedance matching. Simulation results are shown in Fig.17, bandwidth for −10 dB input reflection coefficient is 17.9-22.5 GHz. Antenna gain is 12.8 dBi −13.4 dBi for fractional bandwidth 17%, in-band radiation efficiency of the entire antenna array is higher than 86%.

IV. ANTENNA FABRICATION AND MEASUREMENT

A. MEASUREMENT SETUP AND RELATED ANALYSIS

The antenna is separated into three RO4350B core boards, fabricated with a size of 25.2 mm × 35.1 mm for the top board, and 25.2 mm × 47.6 mm for the middle and bottom board, as in Fig.18. The slot is formed by machinery processing with actual width of 0.9 mm. The fabricated PCB boards

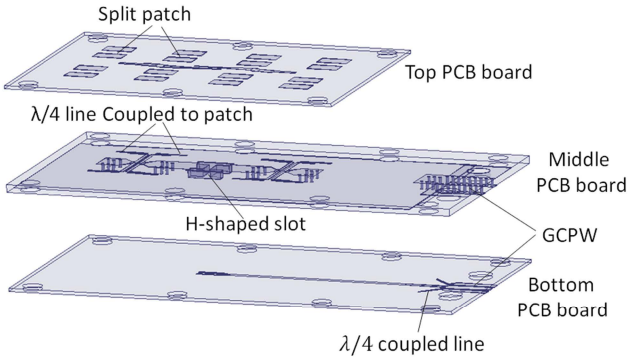

FIGURE 18. Antenna topology with triple PCB boards.

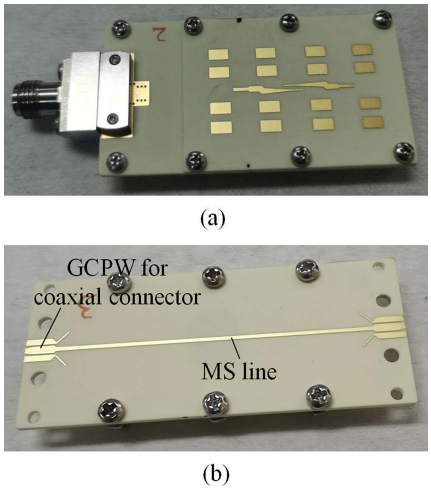

FIGURE 19. (a) Assembled antenna test board (b)Back-to-back test board.

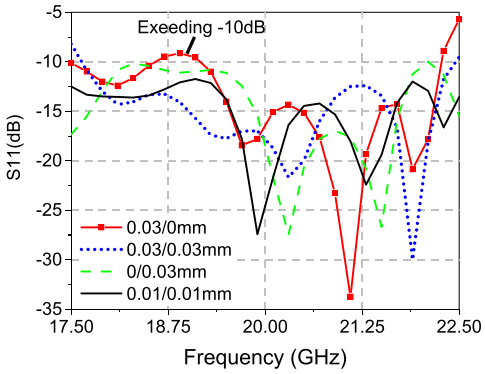

FIGURE 20. Simulated S11 under different air gaps.

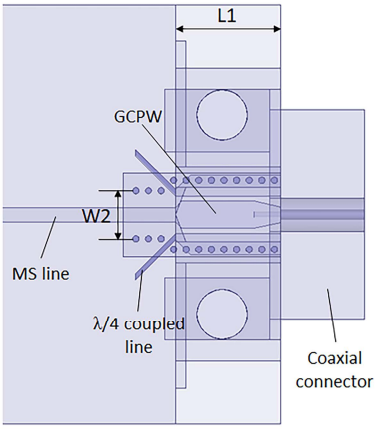

FIGURE 21. Interface design for coaxial connector mounting.

are assembled with screws, as shown in Fig.19(a), a coaxial connector is mounted onto the grounded coplanar waveguide (GCPW) formed on the middle and bottom boards, as in Fig.18.

Simulation shows that the air gaps between the assembled PCB boards have a large impact on input matching, as illustrated in Fig.20, where the coaxial connector model is included during simulation. With the sizes of the two air gaps between the three PCB boards changing between 0 μm and 30 μm, the input reflection coefficient varies drastically, with maximum S11 exceeding -10 dB.

In order to lower the influence of the air gap, no metallization pattern is formed on bottom surface of the top board, or on top surface of the bottom board. The designed interface structure of the coaxial connector is shown in Fig.21, where the MS line is converted into GCPW. No via is available on the bottom PCB board, and the sidewall of the GCPW is formed only by vias on the middle PCB, as in Fig.18. Two $\lambda/4$ coupled lines with length of 2.7 mm are designed to terminate the GCPW side grounds on the lower surface of the bottom board and form a short circuit with the MS line ground on the lower surface of the middle PCB board. The via array of the GCPW on the middle PCB board extends to the left side with width of *W2* equals to 2.3 mm, as in Fig.21, forming an SIW with a very high cut-off frequency, thus wave leakage between the two ground planes on the upper and lower surfaces of the middle PCB board can be suppressed at the junction point of MS line and GCPW. Simulated in-band insertion loss of the transition structure is within 0.3 dB.

B. MEASUREMENT RESULTS

The antenna is measured in the compact-range anechoic chamber, as shown in Fig.22. The horizontal cylindrical quiet zone has a diameter of 2.4 m and length of 3 m. The source antenna in the measurement system is the corrugated horn with gain 6 dBi - 8 dBi. The vector network analyser adopted is Agilent E8363B. Test frequency range is 1 GHz – 40 GHz.

The input reflection coefficient is measured as shown in Fig.23, which exceeds -10 dB at frequency 20.5 - 21.1 GHz with a maximum value of -8.8 dB due to the air gap. The radiation patterns under 20 GHz frequency are depicted in Fig.24. Measured antenna gain is about 11.5 dBi, and is 1 dB lower than the simulation result of 12.47 dBi. Cross polarization on φ =45° plane is also shown in Fig.24. The difference between the co- and cross-polar components in the boresight direction is approximately 20 dB. The cross-polarization level

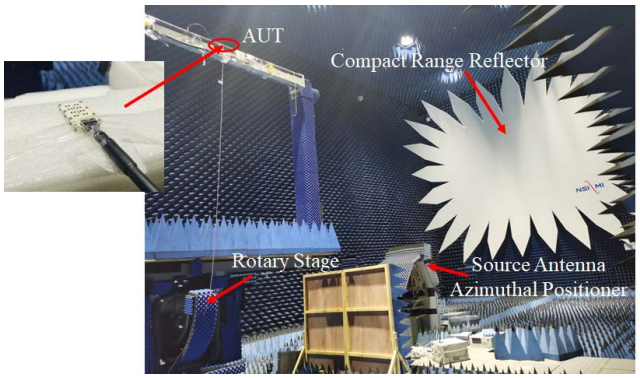

FIGURE 22. Measurement setup in the compact range anechoic chamber.

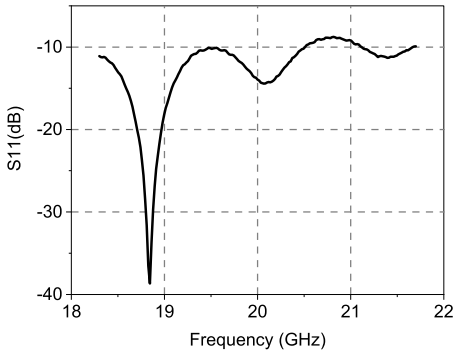

FIGURE 23. Measured input reflection coefficient of the antenna.

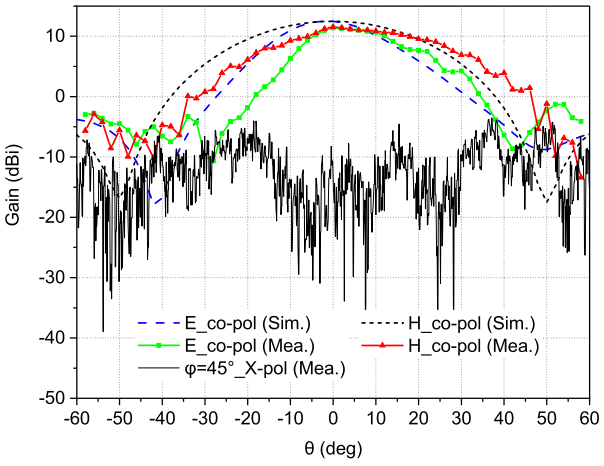

FIGURE 24. Simulated and measured gain at 20GHz.

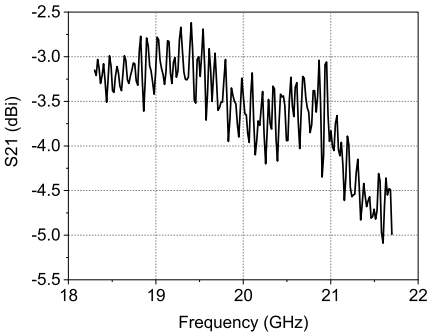

FIGURE 25. Measured insertion loss of the back-to-back test structure.

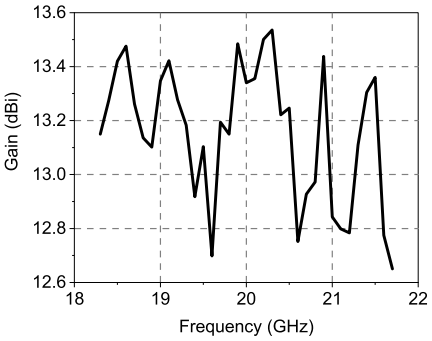

FIGURE 26. Measured gain versus frequency after back-to-back calibration.

is mainly influenced by the measurement setup, such as the circumstances and measurement system noise. In this work no polarization isolation is required, thus cross-polarization characteristic is not restricted; a low cross-polarization level indicates a low power loss.

A back-to-back test structure is designed for the calibration of feeding loss, which includes coaxial connector, GCPW, and MS line, as shown in Fig.19(b); measured insertion loss is −3.43 dB at the frequency of 20 GHz, as depicted in Fig.25, and the resulted feeding loss is −1.72 dB. The in-band gain after calibration is 12.7 dBi - 13.5 dBi, as in Fig.26, which contains losses of vertical slot transition and the conversion balun.

C. COMPARISON

Table 4 summarizes performances of related literatures on organic substrate AiP. Patch antennas with probe feed and aperture-coupled feed are generally adopted. Stacked patches can also be formed for bandwidth enhancement. For probe-fed antenna, parasitic inductor is introduced by the via probe, which influences the bandwidth, if no compensation is applied. Aperture feed has backward electromagnetic leakage that may influence MMIC performance, especially when multiple apertures are formed for array design; extra isolation metal layer is needed. In our work coupling feed is proposed, no series parasitic inductor is formed on the feeding path. Fractional bandwidth of 23% is obtained, which is among the most wideband characteristic in Table 4. Reference [22] has an FBW of 23.3% for the transmitter antenna using aperture-coupled feed, with metallic cavity walls formed by rows of vias around the radiation patch. The MMIC is flip-chip attached onto antenna substrate; the antenna gain is about 5 dBi - 7 dBi. In our work a structure with chip embedded into substrate is formed as in Fig.2, in contrast to that in [22], the antenna feeding network and the chip pad connection wiring are on separate metal layers, a compact 3-dimentional antenna-chip integration is formed, a low package area can be acquired with relatively simple substrate metal layers.

TABLE 4. Comparison between this work and previous related works.

Work	Frequency (GHz)	FBW (%)	Gain (dBi)	Packaging	Properties
[9]	54-65	18.3	--	Fan out	Probe-fed stacked patch
[10]	37.1-41.6	11.4	13.5	Fan out	Probe feed, 2×4 antenna array
[20]	160	12.5	8.8	Flip chip	Probe-fed circular patch, 2×2 antenna array
[21]	28-32	13.3	--	Flip chip	Probe-fed stacked patch, 64 phased array
[22]	53-67	23.3	6	Flip chip	Aperture-coupled feed
[23]	29-31	6.7	7/unit	Flip chip	Aperture-coupled stacked patch, 64 phased array
[24]	89.5-99	10.1	2/unit	Flip chip	Probe-fed stacked patch, 64 phased array
This work	17.9-22.5	23	12.7	Fan out	Coupling feed, 2×4 antenna array

2×4 antenna array is designed with gain over 12.7 dBi; a high antenna efficiency of over 80% is also obtained as illustrated in Fig.17(b), proves the effectiveness of the whole feeding path.

V. CONCLUSION

An antenna topology on organic substrate has been proposed for Antenna-in-Package applications. Patch antenna with coupled feeding is designed for bandwidth enhancement, a series-to-parallel coupled-resonant model is analysed with extracted device parameters. Circuit simulation results coincide with HFSS model performances. $\lambda/4$ coupled line is used for impedance matching. A wideband and low-loss H-shaped slot is adopted for right-angle signal transition. A low-loss conversion balun is designed for interconnection of the MS line to differential MS line in the feeding network. Measurements of the 20 GHz 2×4 radiation array prototype are consistent with the simulation results. The proposed structure realizes a compact and wideband AiP integration that can be suitable for higher frequency mm-wave applications.

REFERENCES

[1] A. Bisognin, N. Nachabe, C. Luxey, F. Gianesello, D. Gloria, J. R. Costa, C. A. Fernandes, Y. Alvarez, A. Arboleya-Arboleya, J. Laviada, F. Las-Heras, N. Dolatsha, B. Grave, M. Sawaby, and A. Arbabian, "Ball grid array module with integrated shaped lens for 5G backhaul/fronthaul communications in F-band," *IEEE Trans. Antennas Propag.*, vol. 65, no. 12, pp. 6380–6394, Dec. 2017.

[2] E. Lacombe, F. Gianesello, A. Bisognin, C. Luxey, D. Titz, H. Gulan, and T. Zwick, "240 GHz antenna integrated on low-cost organic substrate packaging technology targeting high-data rate sub-THz telecommunication," in *Proc. 47th Eur. Microw. Conf. (EuMC)*, Nuremburg, Germany, Oct. 2017, pp. 164–167.

[3] M. Pauli, B. Gottel, S. Scherr, A. Bhutani, S. Ayhan, W. Winkler, and T. Zwick, "Miniaturized millimeter-wave radar sensor for high-accuracy applications," *IEEE Trans. Microw. Theory Techn.*, vol. 65, no. 5, pp. 1707–1715, May 2017.

[4] T. Kamgaing, A. A. Elsherbini, S. N. Oster, B. M. Rawlings, and K. O. Lee, "Ultra-thin dual polarized millimeter-wave phased array system-in-package with embedded transceiver chip," Presented at the IEEE MTT-S Int. Microw. Symp. Dig., Phoenix, AZ, USA, May 2015.

[5] D. Manessis, S. Kosmider, L. Boettcher, M. Seckel, K. Murugesan, U. Maaß, I. Ndip, A. Ostmann, R. Aschenbrenner, M. Schneider-Ramelow, and K.-D. Lang, "Development of innovative substrate and embedding technologies for high frequency applications," Presented at the Eur. Microelectron. Packag. Conf. Exhib., Gothenburg, Sweden, Sep. 2021.

[6] N. Fichtner, U. Siart, and P. Russer, "Antenna bandwidth optimization using transmission line matrix modeling and genetic algorithms," in *Proc. Int. Symp. Signals, Syst. Electron.*, Montreal, QC, Canada, Jul./Aug. 2007, pp. 79–82.

[7] T. Huynh and K. F. Lee, "Single-layer single-patch wideband microstrip antenna," *Electron. Lett.*, vol. 31, no. 16, pp. 1310–1312, Aug. 1995.

[8] P. Lowes, A. Sambell, E. Korolkiewicz, and S. R. Day, "Performance of microstrip patch antenna with electrically thick laminated glass superstrate," *Electron. Lett.*, vol. 30, no. 23, pp. 1903–1905, Nov. 1994.

[9] D. M. Pozar and F. Croq, "Millimeter-wave design of wide-band aperture-coupled stacked microstrip antennas," *IEEE Trans. Antennas Propag.*, vol. 39, no. 12, pp. 1770–1776, Dec. 1991.

[10] W. S. T. Rowe and R. B. Waterhouse, "Investigation into the performance of proximity coupled stacked patches," *IEEE Trans. Antennas Propag.*, vol. 54, no. 6, pp. 1693–1698, Jun. 2006.

[11] K. M. Luk, C. L. Mak, Y. L. Chow, and K. F. Lee, "Broadband microstrip patch antenna," *Electron. Lett.*, vol. 34, no. 15, pp. 1442–1443, Jul. 1998.

[12] I. Ang and B. L. Ooi, "Broadband semi-circle-fed microstrip patch antennas," *IET Microw., Antennas Propag.*, vol. 1, no. 3, pp. 770–775, 2007.

[13] H. F. Pues and A. R. Van de Capelle, "An impedance-matching technique for increasing the bandwidth of microstrip antennas," *IEEE Trans. Antennas Propag.*, vol. 37, no. 11, pp. 1345–1354, Nov. 1989.

[14] W.-J. Wu, B. Ma, Q.-F. Liu, and J. Wang, "A compact ⌈-shaped antenna with filtering characteristics," in *Proc. 7th IEEE Int. Symp. Microw., Antenna, Propag., EMC Technol. (MAPE)*, Xi'an, China, Oct. 2017, pp. 71–73.

[15] L.-H. Wen, S. Gao, Q. Luo, Z. Tang, W. Hu, Y. Yin, Y. Geng, and Z. Cheng, "A balanced feed filtering antenna with novel coupling structure for low-sidelobe radar applications," *IEEE Access*, vol. 6, pp. 77169–77178, 2018.

[16] R. Lovato, T. J. Li, and X. Gong, "Electrically tunable integrated patch antenna with planar filter," Presented at the IEEE Annu. Wireless Microw. Technol. Conf., Cocoa Beach, FL, USA, Apr. 2015.

[17] D. Liu, X. Gu, C. W. Baks, and A. Valdes-Garcia, "Antenna-in-package design considerations for Ka-band 5G communication applications," *IEEE Trans. Antennas Propag.*, vol. 65, no. 12, pp. 6372–6379, Dec. 2017.

[18] J. F. Zuercher, "The SSFIP: A global concept for high-performance broadband planar antennas," *Electron. Lett.*, vol. 24, no. 23, pp. 1433–1435, Nov. 1988.

[19] J. S. Hong, "Coupled-resonator circuits," in *Microstrip Filters for RF/Microwave Applications*, 2nd ed. Hoboken, NJ, USA: Wiley, 2011, ch. 7, pp. 202–215.

[20] B. P. Ginsburg, S. M. Ramaswamy, V. Rentala, E. Seok, S. Sankaran, and B. Haroun, "A 160 GHz pulsed radar transceiver in 65 nm CMOS," *IEEE J. Solid-State Circuits*, vol. 49, no. 4, pp. 984–995, Apr. 2014.

[21] A. Nafe, M. Sayginer, K. Kibaroglu, and G. M. Rebeiz, "2 × 64 dual-polarized dual-beam single-aperture 28 GHz phased array with high cross-polarization rejection for 5G polarization MIMO," in *IEEE MTT-S Int. Microw. Symp. Dig.*, Boston, MA, USA, Jun. 2019, pp. 484–487.

[22] A. Bisognin, A. Arboleya, D. Titz, R. Pilard, D. Gloria, F. Gianesello, and C. Luxey, "Low-cost organic-substrate module for Tx–Rx short-range WiGig communications at 60 GHz," *IEEE Trans. Antennas Propag.*, vol. 69, no. 10, pp. 6196–6208, Oct. 2021.

[23] X. Gu, D. Liu, C. Baks, O. Tageman, B. Sadhu, J. Hallin, L. Rexberg, P. Parida, Y. Kwark, and A. Valdes-Garcia, "Development, implementation, and characterization of a 64-element dual-polarized phased-array antenna module for 28-GHz high-speed data communications," *IEEE Trans. Microw. Theory Techn.*, vol. 67, no. 7, pp. 2975–2984, Jul. 2019, doi: 10.1109/TMTT.2019.2912819.

[24] X. Gu, D. Liu, C. Baks, J.-O. Plouchart, W. Lee, and A. Valdes-Garcia, "An enhanced 64-element dual-polarization antenna array package for W-band communication and imaging applications," in *Proc. IEEE 68th Electron. Compon. Technol. Conf. (ECTC)*, San Diego, CA, USA, May/Jun. 2018, pp. 197–201.

[25] M. Saleem and Y. Saifullah, "Coding artificial magnetic conductor ground and their application to high-gain, wideband radar cross-section reduction of a 2×2 antenna array," *Phys. Status Solidi A*, vol. 218, no. 11, Jun. 2021, Art. no. 2100088.

XUESONG ZHANG received the B.S. degree in microelectronics from Tsinghua University, Beijing, China, in 1992, and the M.E. degree in electronics and communication engineering from Fudan University, Shanghai, China, in 2013. He is currently pursuing the Ph.D. degree with Tsinghua University.

He was with CRMICRO and CSMC, Wuxi, China, from 1992 to 2000. From 2001 to 2003, he was with SinoMOS, Beijing. From 2003 to 2013, he was with SourceCore and Yspringtech, Shenzhen, China, as a Design Engineer for Bluetooth applications. His current research interests include design, modelling, and characterization of antenna-in-package and millimeter-wave radar systems.

QIAN WANG (Member, IEEE) received the Ph.D. degree in materialogy from Tsinghua University, Beijing, China, in 2000. He joined as a Postdoctoral Researcher with the Research Center for Advanced Science and Technology, University of Tokyo, Tokyo, Japan, and the National Institute for Materials Science, Tsukuba, Japan, until 2003. Since 2003, he has been with the Samsung Advanced Institute of Technology, Suwon, South Korea, as a Senior Engineer. From 2006 to 2009, he was with Samsung Semiconductor China Research and Development, Suzhou, China, as a Principle Engineer, and a Leader with the Technology Development Group. Since 2010, he has been an Associate Professor with the Institute of Microelectronics, Tsinghua University. His current research interests include advanced packaging technologies such as SiP, MEMS packaging, and WLP, and packaging reliability and failure analysis.

JIAN CAI (Senior Member, IEEE) received the B.S. degree in materials science and engineering and the Ph.D. degree in metallic materials and heat treatment from Tsinghua University, Beijing, China, in 1993 and 1998, respectively. He joined Tsinghua University in 2002, where he is currently a Professor. His current research interests include advanced packaging, including ultra-fine pitch flip chip, interconnections in 3-D intergration, and high density substrates.